Book of Tutorials and Abstracts

European Microbeam Analysis Society

EMAS 2026

15th

REGIONAL WORKSHOP

TOPICAL CONFERENCE ON ELECTRON BACKSCATTER DIFFRACTION (EBSD)

14 to 17 June 2026
at the
CentraleSupélec, Gif-sur-Yvette, France

Organised in collaboration with:
ICMMO, ENS Paris-Saclay,
Université Paris-Saclay

EMAS
European Microbeam Analysis Society eV
www.microbeamanalysis.eu/

This volume is published by:
European Microbeam Analysis Society eV (EMAS)
EMAS Secretariat
c/o Eidgenössische Technische Hochschule, Department of Earth and Planetary Sciences
Clausiusstrasse 25
8092 Zürich
Switzerland

ISBN 978 90 8227 6992
NUR code: 971 – Materials Science

BASIC CRYSTALLOGRAPHY AND DIFFRACTION FOR EBSD

René de Kloe

AMETEK BV, Gatan (formerly EDAX)
Ringbaan Noord 103, 5046 AA Tilburg, The Netherlands
e-mail: rene.de.kloe@ametek.com

René de Kloe studied geology at Utrecht University in The Netherlands with structural geology and materials science as main subjects. During his MSc thesis on “Deformation and pressure indicators in natural fault rocks from New Zealand” and later during his PhD thesis on "Nanometre scale melt microstructures in experimentally deformed upper mantle rocks", he worked extensively with both scanning and transmission electron microscopes. During his research he started using EBSD and after obtaining his PhD in 2001, he had the opportunity to join EDAX as applications specialist for EBSD and later also EDS at EDAX in Tilburg, The Netherlands. In this position, his focus is on instrument demonstrations, conference and workshop presentations, and customer support. This includes (on-site) training courses, assistance with analytical problems, and scientific collaborations. Although focussed on Europe, his work has brought him to customers and conferences all over the world.

1. *INTRODUCTION*

Electron backscatter diffraction (EBSD) is a scanning electron microscopy (SEM) based technique to measure and characterise the microstructure of crystalline materials. EBSD is based on capturing the diffracted electron signal from a steeply tilted sample in which the crystal lattice is accessible at the surface of the sample. From the diffraction patterns, the phase and/or crystal orientation of the grain in the sample surface may be determined. Because of the dependence on the crystalline nature of any material investigated with EBSD, knowledge of the crystal structure and relevant descriptions for directions and planes is helpful to understand the EBSD signal and subsequent analysis.

This lecture introduces the basic crystallographic and diffraction concepts that are used both for the EBSD pattern analysis and during post-processing of collected datasets. The presented information is not intended to be a treatise on crystallography, instead it is focussed on the concepts that are directly related to EBSD patterns and their analysis.

2. *CRYSTAL DEFINITIONS*

A crystal can be defined as a solid composed of atoms arranged in a pattern that is periodic in three dimensions. This periodic structure is then described as a crystal lattice, which is an array of points in space arranged such that each point has identical surroundings (Fig. 1).

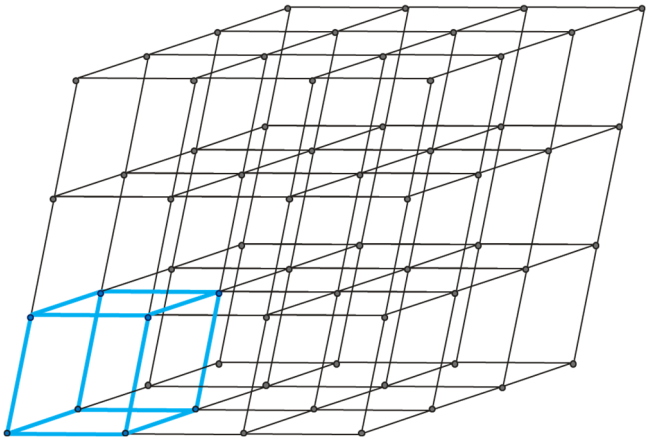

The lattice points are used to define planes and directions in the crystal:

- Crystal plane: A set of lattice points that lie in one plane
- Crystal direction: A set of lattice points that lie along a line
- Crystal axes: The reference vectors that define the unit cell

Figure 1. Crystal lattice with unit cell.

Within the crystal lattice a single unit can be identified that can be repeated in all directions to enlarge the crystal. This parallelepiped containing just one lattice point is the primitive unit cell. *Note that lattice points are not limited to single atoms. Each lattice point may contain multiple atoms, as long as all lattice points are identical.*

The dimensions of the unit cell define the lattice parameters of the crystal (Fig. 2).

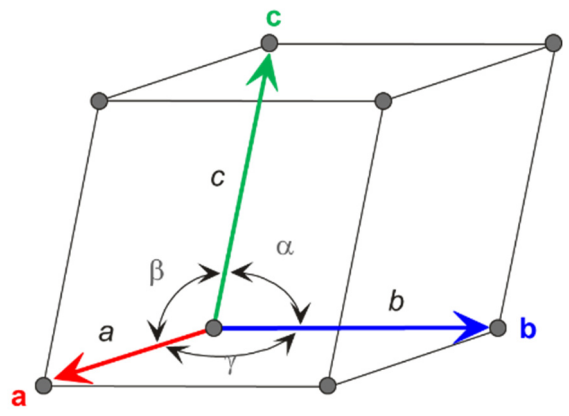

a, **b,** & **c**	Vectors defining the unit cell (crystallographic axes)
a, *b,* & *c*	The lengths of these vectors
α, β, & γ	The angles between these vectors

Figure 2. Unit cell dimensions with lattice parameters.

All crystalline materials can be divided into only seven crystal systems by their lattice parameter relationships. Table 1 below summarises the minimum symmetry elements and lattice parameter relationships for the crystal systems.

Table 1. Crystal system symmetry and lattice parameter relationships (with no. of point groups for each system).

Crystal Systems (32)	Rotation Axes				Mirror Planes	Center of Inversion	Lattice Parameter Relationships	
	2	3	4	6				
Triclinic (2)	-	-	-	-	-	yes	$a \neq b \neq c$	$\alpha \neq \beta \neq \gamma$
Monoclinic (3)	1	-	-	-	1	yes	$a \neq b \neq c$	$\alpha = \gamma = 90° < \beta$
Orthorhombic (3)	3	-	-	-	3	yes	$a \neq b \neq c$	$\alpha = \beta = \gamma = 90°$
Trigonal* (5) (Rhombohedral)	3	1	-	-	3	yes	$a = b = c$	$\alpha = \beta = 90°, \gamma = 120°$
Tetragonal (7)	4	-	1	-	5	yes	$a = b \neq c$	$\alpha = \beta = \gamma = 90°$
Hexagonal (7)	6	-	-	1	7	yes	$a = b \neq c$	$\alpha = \beta = 90°, \gamma = 120°$
Cubic (5)	6	4	3	-	9	yes	$a = b = c$	$\alpha = \beta = \gamma = 90°$

A simplified illustration of the changes between the crystal systems can be made by progressive changes in the unit cell shape (Fig. 3a). Based on a rectangular arrangement of the lattice points, five of the crystal systems can be defined as a sequence from high to low symmetry geometries. For cubic crystals the **a-**, **b-**, and **c**-axes are equally long and perpendicular to each other → stretching the **c**-axis transforms the shape into tetragonal → additional stretching of the **b**-axis changes the crystal to orthorhombic → tilting the **c**-axis in the **b**-direction defines monoclinic → and finally skewing the remaining 90° angles makes triclinic.

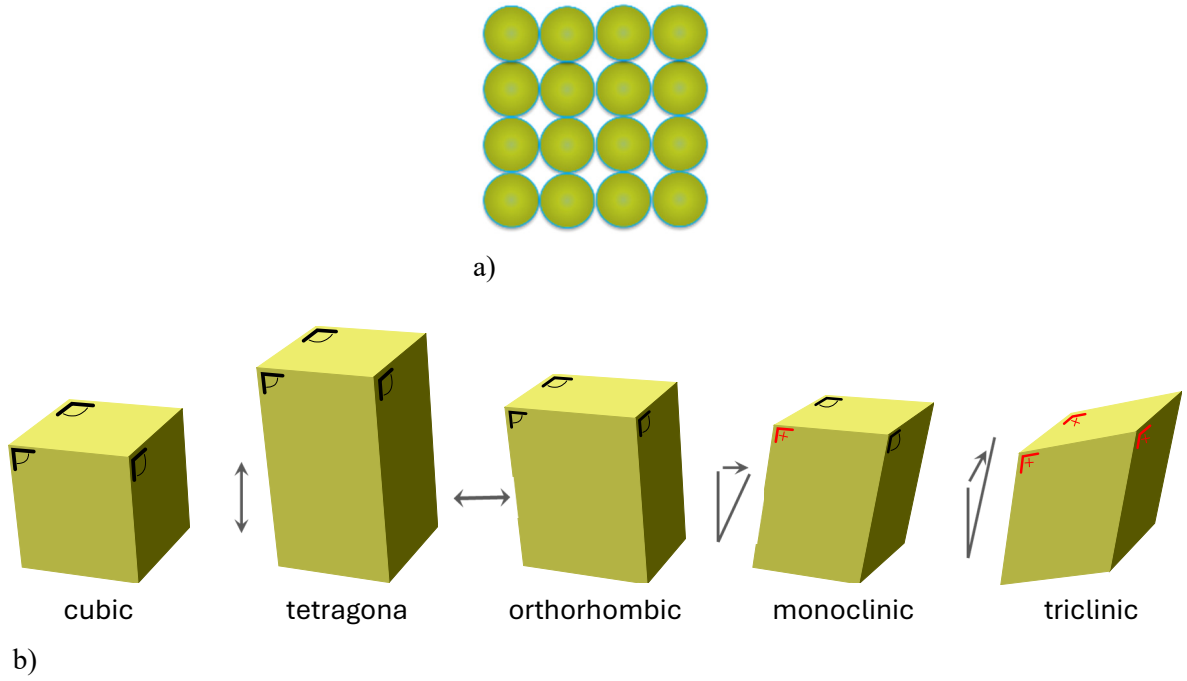

Figure 3. a) A simplified illustration of the changes between the crystal systems can be made by progressive changes in the unit cell shape. b) Change from cubic to triclinic crystal shape.

Similarly, the remaining two crystal systems, hexagonal and trigonal can be illustrated based on a hexagonal configuration of lattice points where a distortion of the hexagonal basal plane reduces the six-fold to the three-fold symmetry of trigonal crystals (Fig. 4).

3. *DIRECTIONS [uvw] AND PLANES (hkl)*

Directions and planes in crystals use the unit cell as a starting point with the a-, b-, and c-vectors as unit length. All direction vectors and lattice planes must connect lattice points so that the indices are always shown as integers. Crystal directions are indicated as [*uvw*] and planes as (*hkl*).

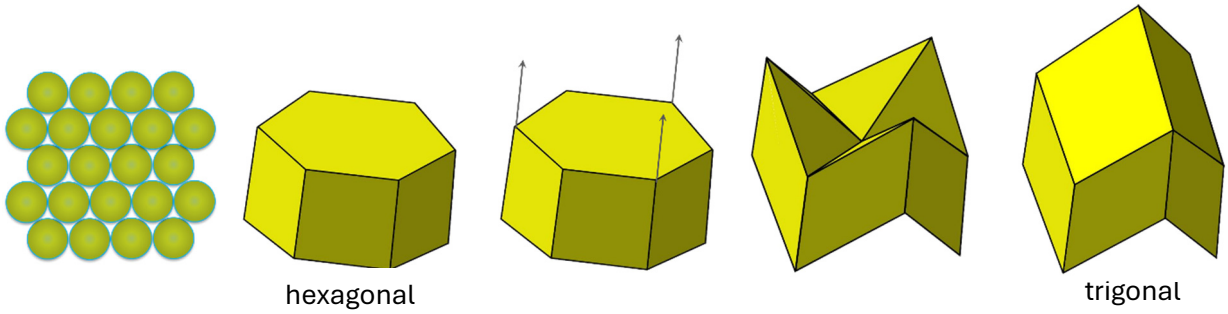

Figure 4. Highest symmetry is hexagonal with 6-fold rotation at 60° intervals - "push" basal plane up every 120° to break the hexagonal symmetry and obtain three-fold trigonal symmetry.

For example, the vector OA in Fig. 5 can be described as spanning one unit length along the **a**-axis, one unit length along **b**, and half a unit length along **c** or [1,1,1/2]. As the direction needs to connect lattice points, the digits are then multiplied to remove the fraction, and the crystal direction [*uvw*] is given as [221]. The square brackets used indicate that [221] is a specific crystal direction. When a set of crystallographically equivalent directions is indicated, the indices are shown with triangular brackets <221>. This is the three-digit Miller indices notation used for the five crystal systems shown in Fig. 3.

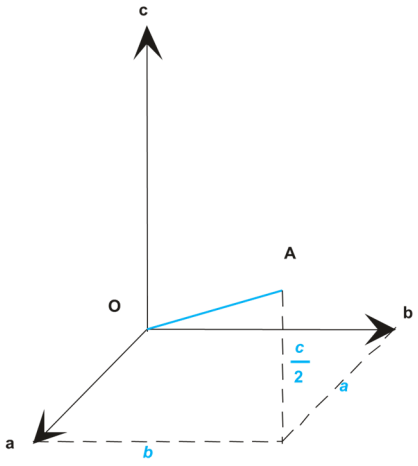

Figure 5. Crystal direction.

Due to the higher symmetry in the basal plane, four-digit Miller-Bravais indices are typically used for hexagonal and trigonal crystals. For these crystals the unit cell is defined by three co-planar axes $\mathbf{a}_1$, $\mathbf{a}_2$, $\mathbf{a}_3$ in the basal plane and a perpendicular **c**-axis (Fig. 6). A direction is then given as [*uvtw*] where t = -(u+v).

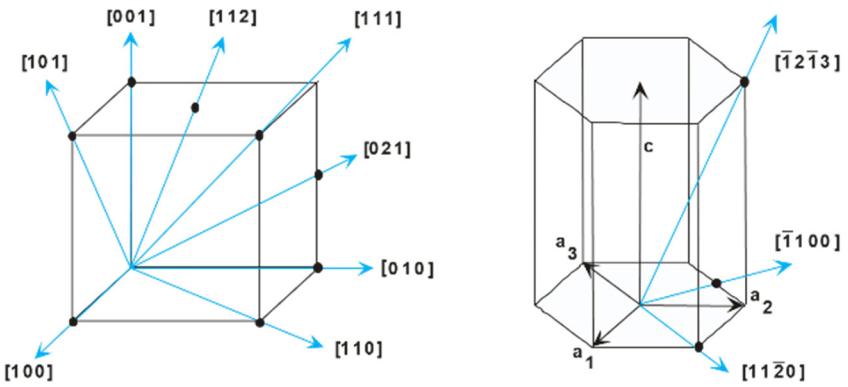

Figure 6. Example crystal directions in cubic and hexagonal crystals.

Lattice planes are described in a similar way, but reciprocal. Indices for a specific plane are now (*hkl*) – using round brackets. Sets of equivalent planes are indicated with {*hkl*} and in the unit cell these are defined as *a*/*h*, *b*/*k*, *c*/*l*. An easy way to visualise this is that the indices indicate how many interplanar spacings are present in a unit length. The higher the index, the closer together the lattice planes are along that axis. For example, the (112) plane in Fig. 7 cuts one unit length from *a*, one from *b*, and ½ from *c* such that there are two plane intersections along the c-axis.

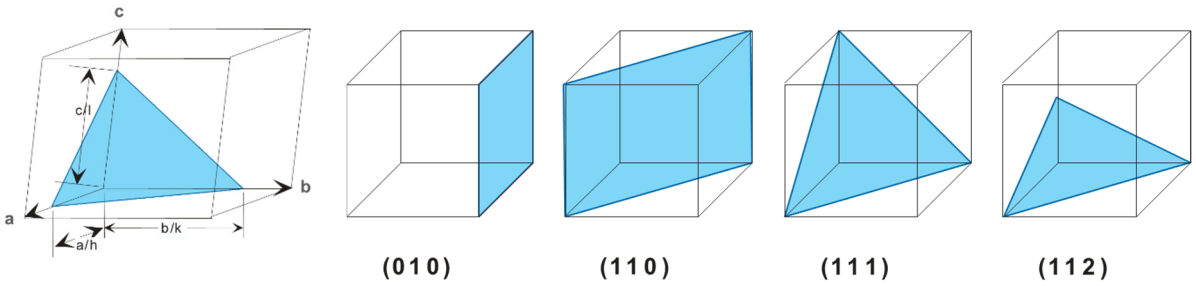

Figure 7. Crystal lattice planes – Miller indices.

As for directions, lattice planes in hexagonal and trigonal crystals use the four-digit Miller-Bravais indices notation (Fig. 8). A plane is then given as [*hkil*] where I = -(h+k).

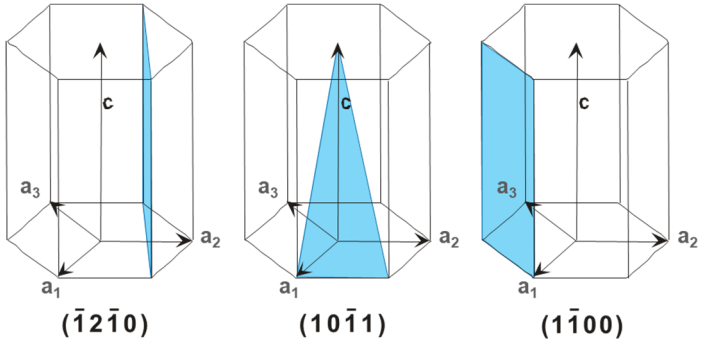

Figure 8. Crystal lattice planes – Miller-Bravais indices.

In EBSD analysis, the distance between the crystal lattice planes and the kind of atoms on each plane are important. They directly affect the appearance of the EBSD patterns where the bands are representations of the lattice planes (Fig. 9).

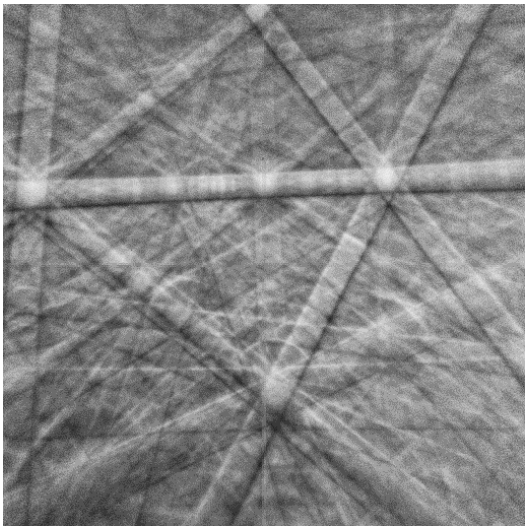

Figure 9. Kyanite EBSD pattern.

The d-spacings determine the band widths in the pattern and the density and atomic number of the atoms on each plane influence its overall brightness.

The correlation between d-spacing and atomic density is illustrated in the 2D crystal lattices in Fig. 10. The planes with the largest d-spacing (10) have the smallest distance between the atoms whereas the (15) planes have a close spacing but very large distance between points making it unlikely to result in a significant signal in an EBSD pattern. This is why most bands identified in EBSD patterns represent low-index planes.

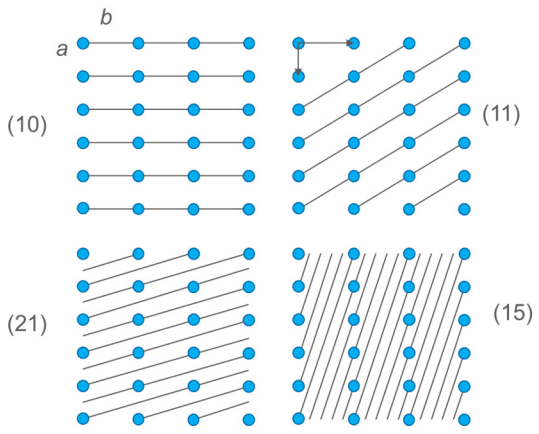

Figure 10. Planes on 2D crystal lattice.

The d-spacings can be calculated using the following equations:

$$d_{hkl} = a(h^2 + k^2 + l^2)^{-1/2} \text{ (cubic crystals) or}$$
$$d_{hkl} = V[h^2b^2c^2\sin^2\alpha + k^2a^2c^2\sin^2\beta + l^2a^2b^2\sin^2\gamma + 2hlab^2c(\cos\alpha\cos\gamma - \cos\beta) + 2hkabc^2(\cos\alpha\cos\beta - \cos\gamma) + 2kla^2bc(\cos\beta\cos\gamma - \cos\alpha)]^{-1/2}$$
$$\text{with } V = abc[1 - \cos^2\alpha - \cos^2\beta - \cos^2\gamma\ 2\cos\alpha\cos\beta\cos\gamma]^{1/2}$$

Crystal directions are not directly visible in EBSD patterns but are often indicated in the indexing overlay. The indices displayed on band intersections in patterns represent zone axes or intersection directions of multiple lattice planes (Fig. 11).

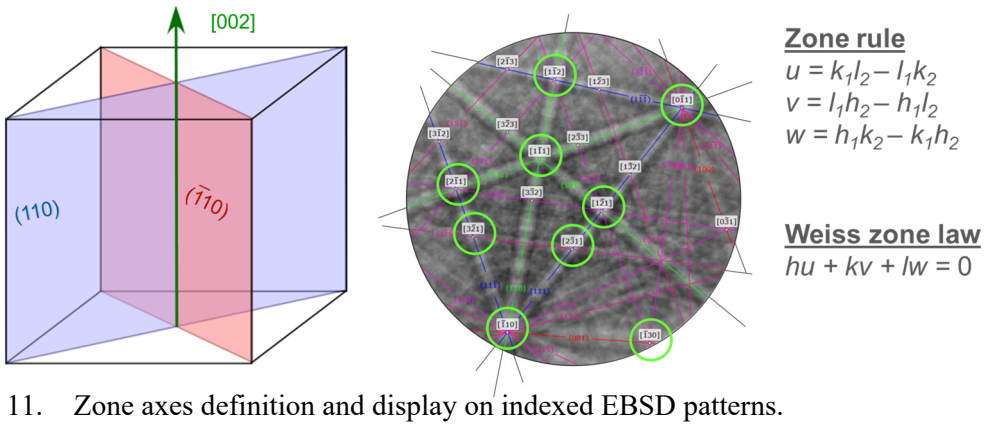

Figure 11. Zone axes definition and display on indexed EBSD patterns.

4. *CRYSTAL SYMMETRY*

The geometry of the bands in an EBSD pattern reflects the point group symmetry of the crystal. This point group symmetry can be described as the set of rotations which when applied to the crystal lattice rotate the lattice into an orientation indistinguishable from the original orientation (Fig. 12). One point in the unit cell does not move. For example, for a cubic symmetry the rotation axes can be defined as shown in Fig. 12.

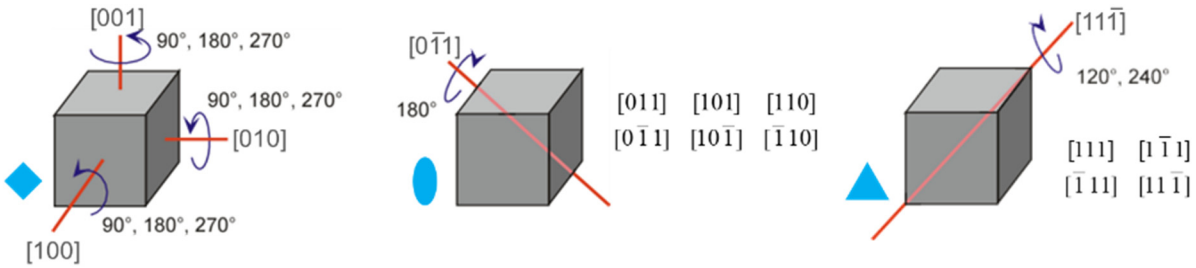

Figure 12. Rotation axes for the cubic $m\bar{3}m$ point group.

Three four-fold axes around <001>, six 2-fold axes around <110>, and four three-fold axes around <111>. These rotation axes and accompanying mirror planes can also be recognised directly in EBSD patterns (Fig. 13).

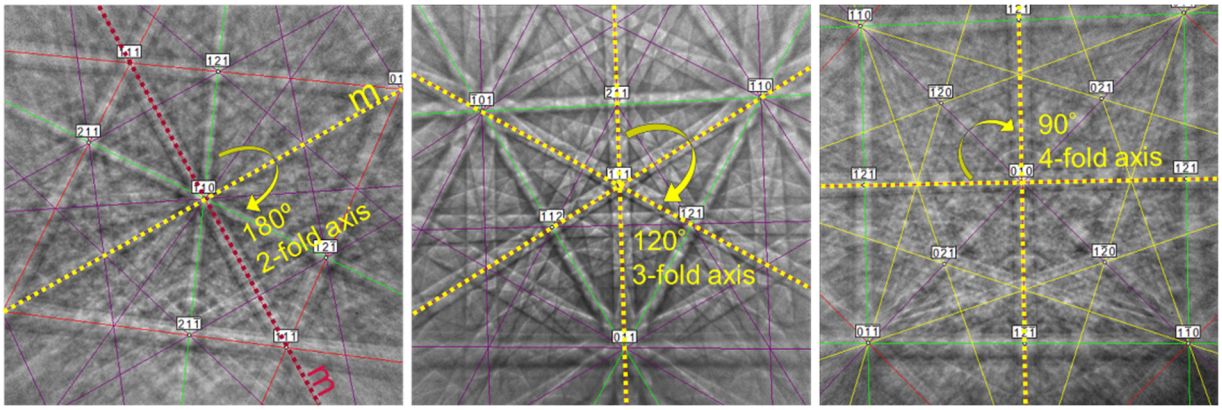

Figure 13. Recognisable mirror planes and rotation axes in EBSD patterns.

Each of the seven crystal systems possesses a number of point symmetry elements characteristic of the system. The total number of possible combinations is 32, called the 32 point-groups. Note that atomic groups at the lattice points may reduce that symmetry or introduce new symmetry elements.

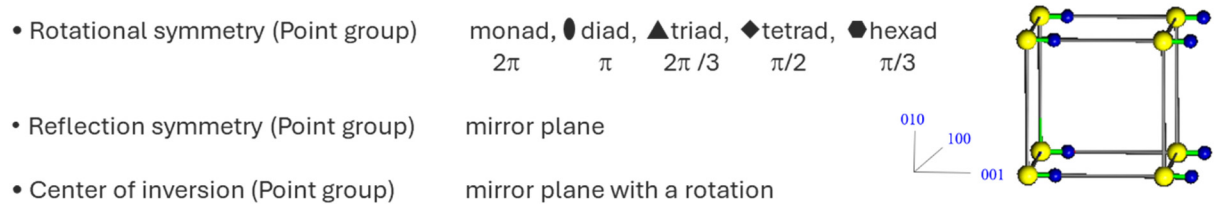

Additional symmetry elements can be recognised that add "movement" to a point group such that all points in the unit cell are shifted from their original position. This defines the 230 space groups. These translations, screw axes, and glide planes do not change the geometry of the bands in the EBSD patterns, but instead control which bands are visible. Certain reflections may be "forbidden" due to destructive interference of the diffracting electrons (Fig. 14). The space group information is also used to locate all atom positions in the unit cell without having to specify each atom individually.

Recognising rotational and mirror symmetry in EBSD patterns is not always obvious due to the projection geometry on the EBSD detector. The symmetry would be preserved in a pattern when the detector can be placed parallel to the sample surface and the projection is centred. However, the conventional EBSD detector geometry is a downward point projection on an often tilted detector which causes a distortion towards the bottom of the pattern (Fig. 15). In order to identify

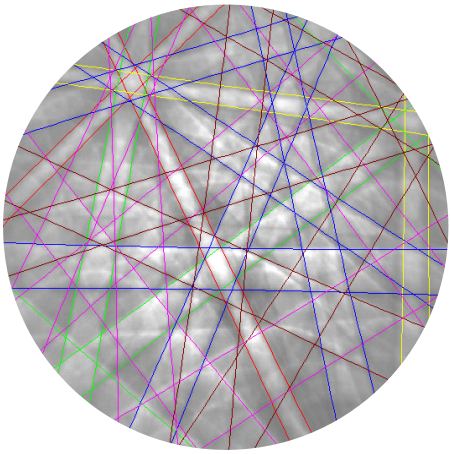

Color	(hkl)	*d*-spacing
	111	2.31
	200	2.00
	220	1.41
	311	1.21
	331	0.92
	042	0.89

Figure 14. Indexing overlay on Ni EBSD pattern with indicated lattice planes. The (100), (110), and (021) reflections are forbidden. Instead, the wider higher order (200), (220), and (042) reflections are displayed.

the true angles between the lattice planes for indexing, a correction needs to be applied. This is the purpose of the EBSD pattern calibration which identifies the position where the electrons hit the detector perpendicularly (the pattern or projection centre) and allows reconstruction of the angles in the crystal.

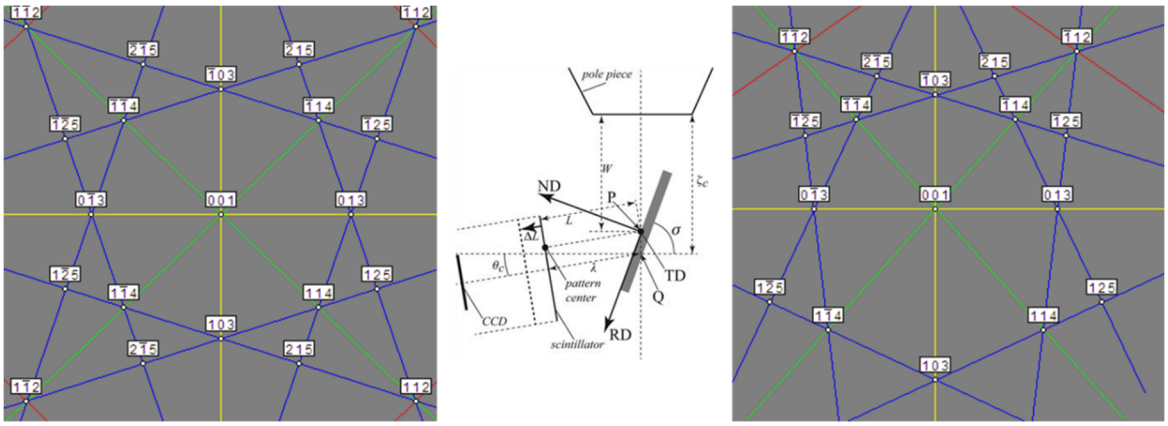

Figure 15. Simulation of parallel and gnomonic projection of EBSD bands.

5. *ELECTRON BACKSCATTER DIFFRACTION*

Electron diffraction can be described by Bragg's law, $n\lambda = 2d_{hkl} \sin\theta$ which links a beam of incoming (electron) radiation with wavelength λ onto a periodic structure with spacing d to the angle θ to allow outward scattering with the same angle (Fig. 16).

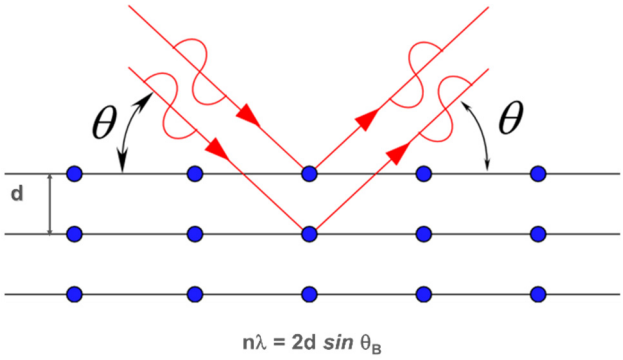

Figure 16. Schematic of diffraction with a parallel beam.

This description shows a parallel beam to obtain consistent scattering on a given lattice plane. However, in the SEM we work with a focussed (convergent) beam on the sample and EBSD patterns are formed by a two-step diffraction process (Fig. 17):

1. The convergent beam enters the sample and at a certain depth forms a "virtual point source" from which electrons are scattered inelastically in all directions → this forms the typical electron interaction volume for EDS analysis.
2. Only the electrons from the virtual point source that travel towards the tilted sample surface and scatter elastically on the atomic layers on the way out carry the EBSD band information.
3. The depth of the virtual point source defines the information depth and lateral resolution of EBSD measurements.

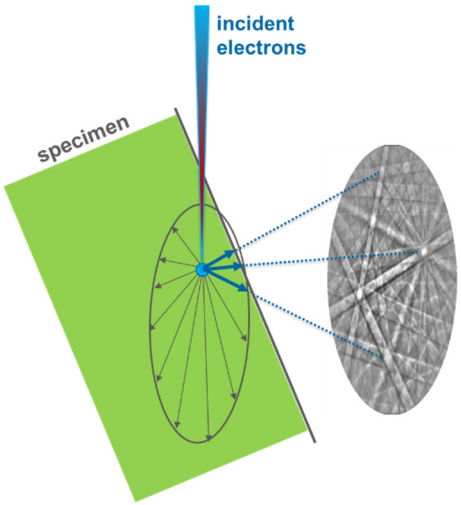

Figure 17. Two-step diffraction in EBSD geometry.

From the virtual point source, cones of electrons diffract from the top and bottom of the lattice planes (Fig. 18). The intersection of these cones with the EBSD detector form the edges of the EBSD bands so that the band width corresponds to twice the Bragg angle θ. Because the Bragg angle in electron diffraction is typically very small, the hyperbolic band edges appear almost parallel to each other and are often treated as straight lines.

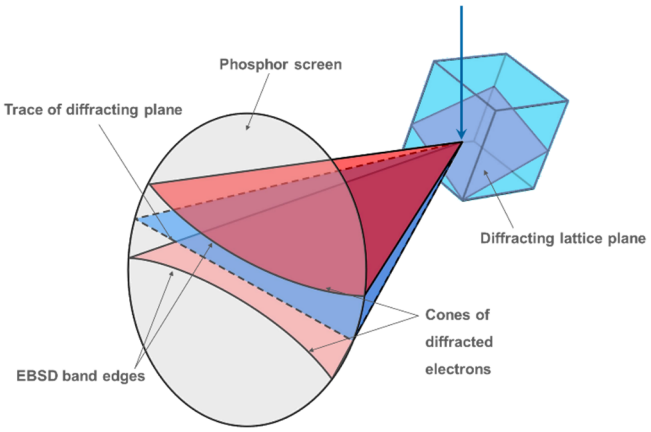

Figure 18. Band edges are formed by the intersection of diffraction cones from the top and bottom of the crystal lattice lanes with the EBSD detector.

As the Bragg angle is linked to the wavelength of the electrons, the opening angle of the cones and thereby the band width changes with the SEM kV setting. The zone axes positions do not change (Fig. 19).

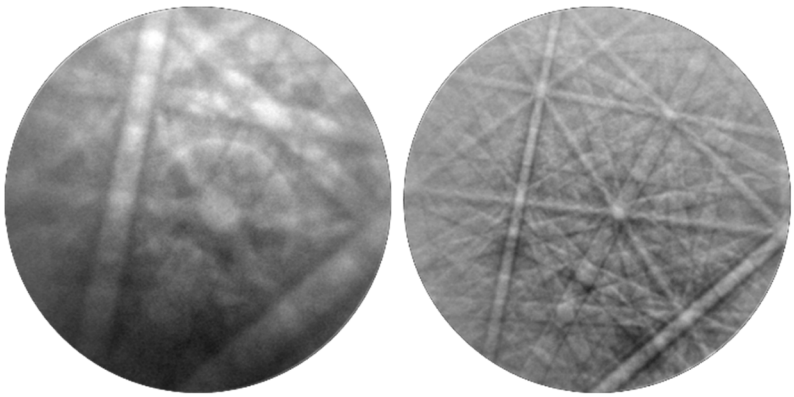

Figure 19. NiAs EBSD patterns collected at 7 kV and 50 kV.

The nature and density of the atoms on each lattice plane affects the probability that diffraction occurs. The resulting diffraction intensity on each crystal lattice plane is described by a structure factor which can be seen as a backscatter coefficient for individual lattice planes. Using the

space group information, all atomic positions are located and with the atomic scattering factor the structure factor can be determined (Fig. 20). The structure factor can be used to select the strongest reflectors for lattice planes to be used for EBSD pattern indexing.

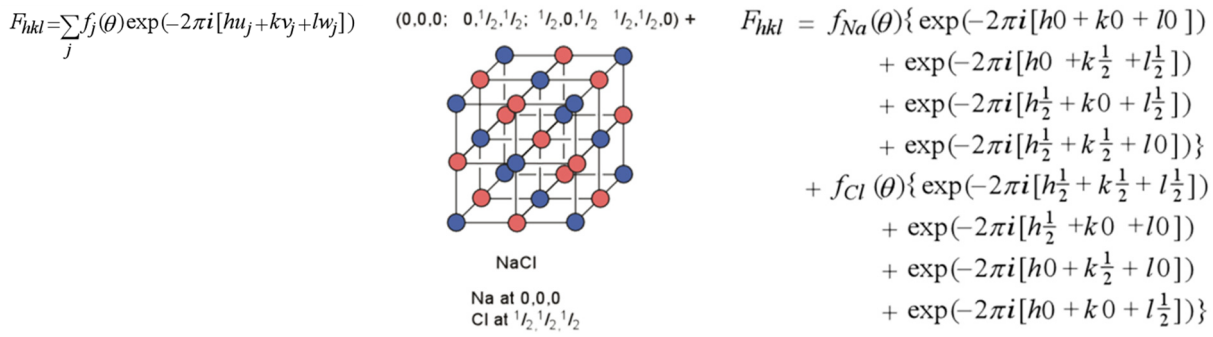

Figure 20. Calculation of the structure factor for lattice planes in the NaCl structure.

The effect of the atomic scattering factor can be seen in unprocessed EBSD patterns (Fig. 21). At identical EBSD conditions, the diffraction signal of heavier elements is brighter and projects higher on the EBSD detector.

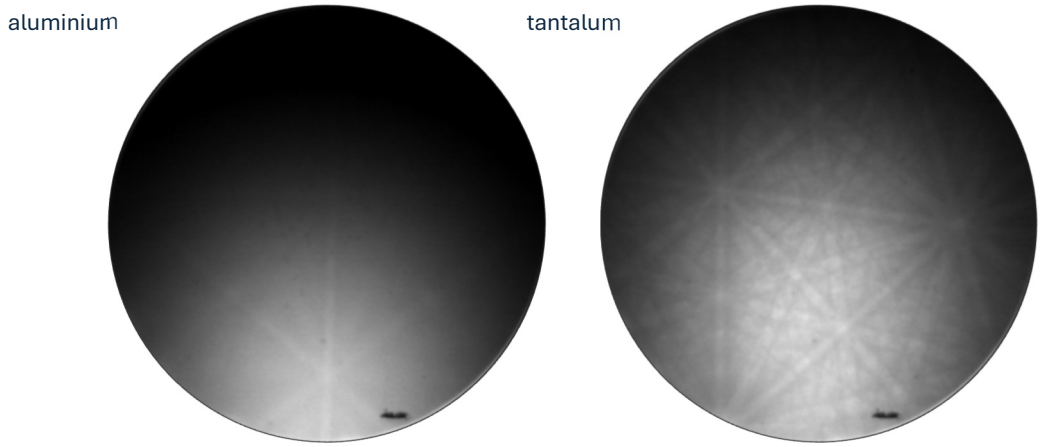

Figure 21. Unprocessed EBSD patterns of Al and Ta at identical conditions.

The information volume also affects the appearance of EBSD patterns in deformed materials. A perfect crystal shows consistent diffraction angles along lattice planes which results in sharp band edges. When lattice defects cause bending of the lattice within the interaction volume, the diffraction cones change in direction and the range of cone orientations mix at the band edges which become unsharp (Fig. 22). This effect can be exacerbated when the electron beam diameter is relatively large (e.g., on W SEMs) or when the sample surface contains deformation artefacts from polishing.

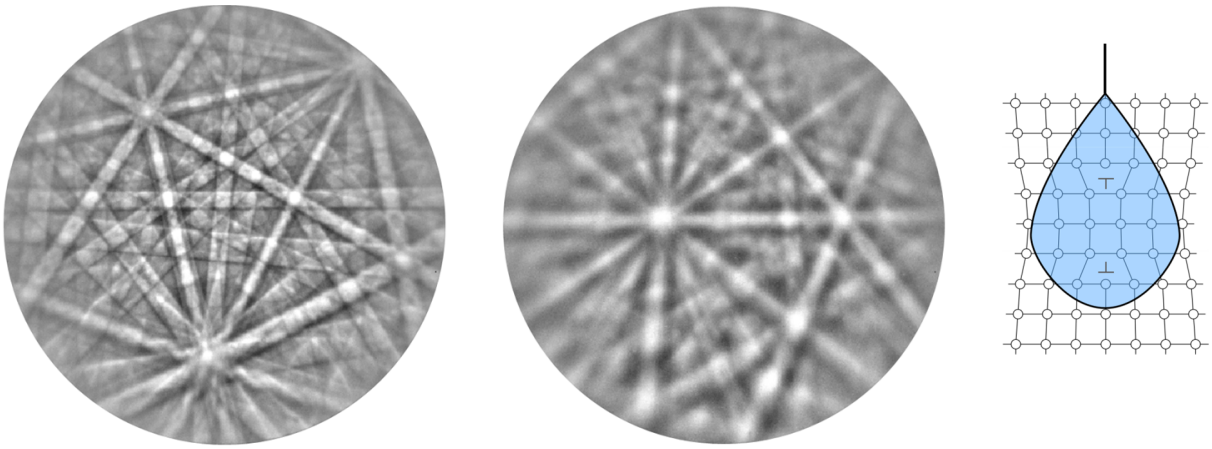

Figure 22. Difference in EBSD pattern sharpness caused by lattice defects. Left: Undistorted lattice; Right: deformed lattice.

As can be seen in the unprocessed patterns in Fig. 21, the intensity of the diffracted bands is quite low. This is caused by the contribution of electrons that are simply scattered from the sample surface without being diffracted on the lattice planes. The fraction of electrons that have been diffracted and contribute to the bands can be estimated from a 3D intensity plot of an unprocessed EBSD pattern (Fig. 23). On an unprocessed pattern the actual band intensity is typically only 5 – 20 % of the total signal. The ratio further depends on density, crystal quality, and surface condition.

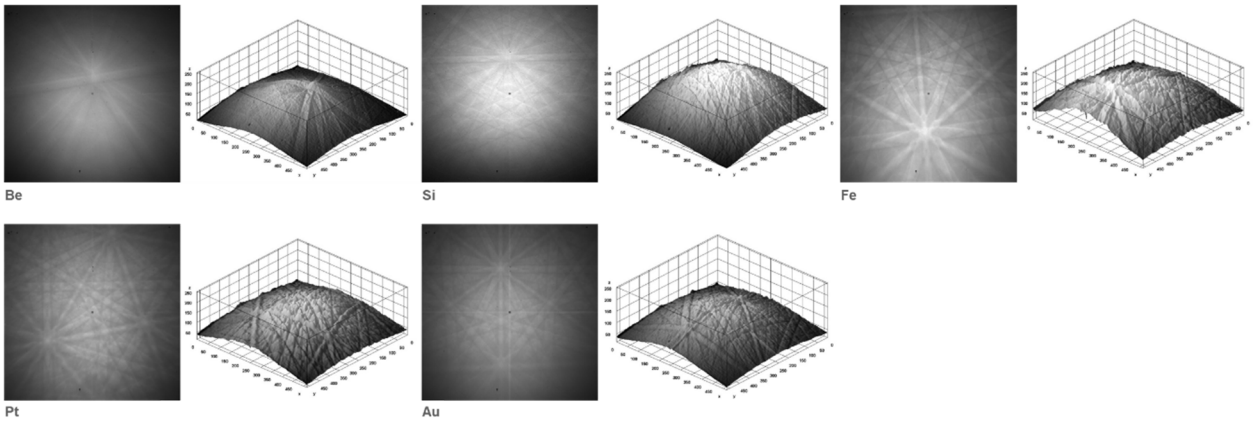

Figure 23. EBSD patterns of Be, Si, Fe, Pt, and Au with 3D intensity plots.

It is this band to background ratio together with the intensity gradient in the patterns that dictates the need for image processing and background removal. One method is to collect an average pattern from a large number of grains such that you only see the intensity gradient and no bands anymore (Fig. 24). This background pattern can then be removed using a number of image processing routines to prepare the pattern for orientation determination by indexing (Fig. 25).

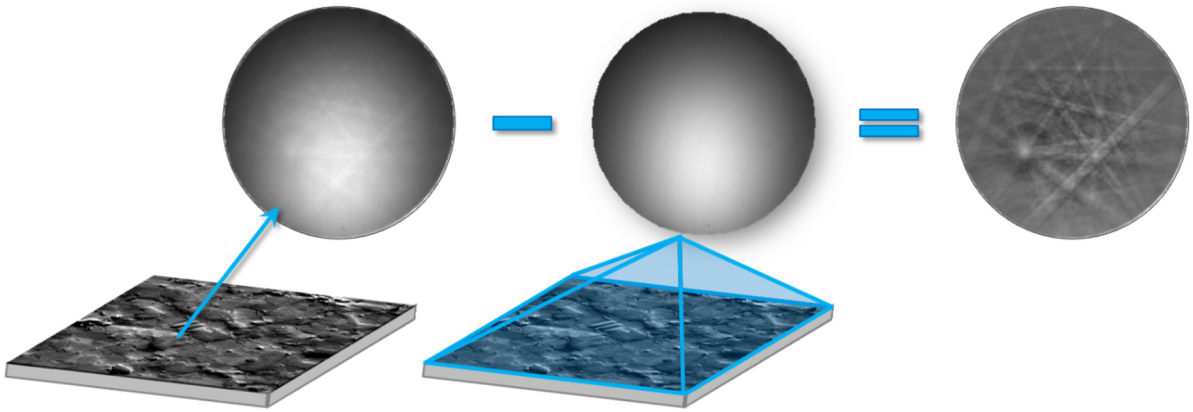

Figure 24. Background correction sequence.

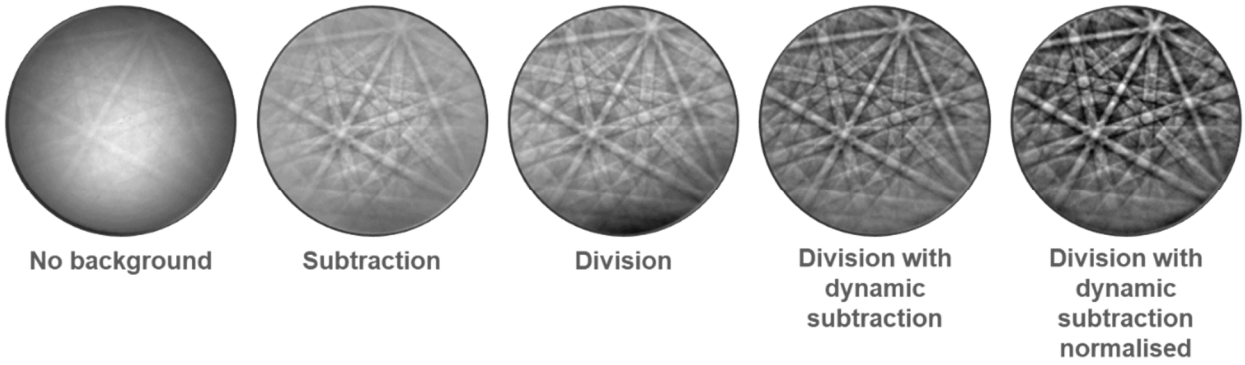

Figure 25. Different EBSD background processing results.